

Complex network modeling of EEG band coupling in dyslexia: An exploratory analysis of auditory processing and diagnosis

Nicolás J. Gallego-Molina^{a,c,*}, Andrés Ortiz^{a,c}, Francisco J. Martínez-Murcia^{b,c}, Marco A. Formoso^{a,c}, Almudena Giménez^d

^a Department of Communications Engineering, University of Málaga, Spain

^b Department of Signal Theory, Networking and Communications, University of Granada, Spain

^c Andalusian Data Science and Computational Intelligence Institute (DaSCI), Spain

^d Department of Developmental Psychology, University of Málaga, Spain

ARTICLE INFO

Article history:

Received 29 July 2021

Received in revised form 1 December 2021

Accepted 30 December 2021

Available online 5 January 2022

Keywords:

Dyslexia diagnosis

EEG

Complex network

Graph analysis

PAC

ABSTRACT

Complex network analysis has an increasing relevance in the study of neurological disorders, enhancing the knowledge of brain's structural and functional organization. Network structure and efficiency reveal different brain states along with different ways of processing the information. This work is structured around the exploratory analysis of the brain processes involved in low-level auditory processing. A complex network analysis was performed on the basis of brain coupling obtained from electroencephalography (EEG) data, while different auditory stimuli were presented to the subjects. This coupling is inferred from the Phase-Amplitude coupling (PAC) from different EEG electrodes to explore differences between control and dyslexic subjects. Coupling data allows the construction of a graph, and then, graph theory is used to study the characteristics of the complex networks throughout time for control and dyslexic subjects. This results in a set of metrics including clustering coefficient, path length and small-worldness. From this, different characteristics linked to the temporal evolution of networks and coupling are pointed out for dyslexics. Our study revealed patterns related to Dyslexia as losing the small-world topology. Finally, these graph-based features are used to classify between control and dyslexic subjects by means of a Support Vector Machine (SVM).

© 2022 The Author(s). Published by Elsevier B.V. This is an open access article under the CC BY license (<http://creativecommons.org/licenses/by/4.0/>).

1. Introduction

The analysis of complex networks has been used in many fields related to social sciences, physics and information technology. It is based on graph theory, and provides meaningful and easily computable measures to explore connectivity between nodes. Since networks are commonplace in the brain, the application of these advances to neuroscience was just a matter of time.

Complex network analysis provides meaningful ways of quantifying the structural and functional brain systems [1], making easier to explore structural-functional connectivity relationships of the brain processes. It is, therefore, a promising technique to reveal connectivity abnormalities in neurological and psychiatric conditions [2]. There are many examples in the literature of the use of complex network analysis to investigate brain networks. For example, many studies analyze complex networks of physiological and pathological brain aging such as Alzheimer's

disease [3–6]. Other works employ functional connectivity and complex network analysis in epilepsy such as [7], where electroencephalography (EEG)-based functional connectivity of six pediatric patients were analyzed to detect patterns related to childhood absence epilepsy. Or the case of [8], where researchers applied graph theoretical analysis to magnetoencephalography (MEG) functional connectivity networks to study schizophrenia.

Such a success makes it an optimal choice for studying the brain connectivity underlying some other conditions. This is the case of Developmental Dyslexia (DD), a condition causing learning disability which affects between 5% and 13% of the population [9]. DD is characterized by poor phonemic awareness and phonological processing [10]. It manifests with symptoms such as slow and inaccurate reading (poor word decoding, low fluency, difficulties in rhyming, frequent misspellings), illegible handwriting, and letter migration or inversion. DD is not related to mental age or inadequate schooling. However, it can be a significant factor in school failure and have an important impact on children's self-esteem [10]. Early diagnosis is essential to help dyslexic children develop intellectually and personally, applying preventive strategies to improve oral language [11].

* Corresponding author at: Department of Communications Engineering, University of Málaga, Spain.

E-mail address: njgm@ic.uma.es (N.J. Gallego-Molina).

Early DD diagnosis is a relevant area of study that may benefit from applying complex network analysis of the brain. In this regard, many studies have performed functional connectivity analyses of functional Magnetic Resonance Imaging (fMRI) data [12–15]. Despite methodological heterogeneities, the analysis of brain networks reveals a general trend towards highly clustered and highly integrated structures, consistent with a small-world network topology across studies [16].

fMRI is by far the most extended technique in brain connectivity. However, it is slow, has a coarse temporal resolution, and it is fairly expensive. Moreover, it would be very difficult to apply to children, the target population for early DD diagnosis. On the contrary, EEG is a suitable candidate. EEG is a fast, cost-efficient and non-invasive technique, with high temporal resolution, that could be easily applied to pre-readers. The usage of EEG is common in sleep and epilepsy studies. In [17] and [18] EEG is used to study sleep stage and perform a classification with a Support Vector Machine (SVM) classifier. Sharma et al. [19] employs features extracted from single-channel EEG to the identification of insomnia. Epilepsy studies work with EEG to diagnose epileptic seizures. They extract features from the EEG signals and classify them. In [20] a SVM is trained with spectral-temporal features for EEG seizure onset detection, and Darjani and Omranpour [21] extract features from the phase space of the EEG signals for epileptic seizure classification.

EEG has also been successfully applied to DD. In [22] and [23], EEG resting state networks are analyzed to study differences in the topological properties. The functional connectivity of reading neural network in DD was studied in [24] to assess differences in the topological properties between groups before and after a visual training. A graph theory analysis was performed in [25] to compare EEG functional connectivity networks in typical and dyslexic readers during an audiovisual task, and in [26] to study the effect of training with visual tasks in the functional connectivity in DD. In the same line, [27] applied a graph-based approach to evaluate functional connectivity in DD. Also, EEG connectivity analysis was used in [28] to investigate the relation between reading dysfluency and dysfunctional connectivity in the brain's networks. Even deep learning strategies, such as Denoising Autoencoders, have been applied to extract composite measures from connectivity of EEG signals in DD [29]. Last, but not least, [30] used Phase-Amplitude Coupling (PAC) techniques to evaluate the neural quality of speech encoding.

In the present work, we used complex network analysis to examine the differences between dyslexics and controls using network characteristics. This analysis relies on Phase-Amplitude Coupling measures and is focused on the exploratory analysis of the brain processes. With that in mind, the relations described with PAC between frequency bands are used to construct the networks including information of the intra-electrode PAC through time for every subject. To this end, PAC measured and graph theory provide a basis to analyze and quantify the differences. Finally, these network characteristics are used as features to train a SVM classifier.

The main contributions of this paper are threefold. Firstly, the methodology is based on the use of novel non-speech and non-interactive stimuli. These low-level auditory stimuli were provided by the psychologists within the Leeduca Project. The dataset that has a similar sample size to previous studies such as [31–33], includes typically developing and dyslexic children. The stimuli seek to exhibit the atypical oscillatory sampling at temporal rates of amplitude modulation in children with dyslexia, based on the Temporal Sampling Framework (TSF) proposed by Goswami [34] that states that the phonological difficulties could be caused by abnormal oscillatory entrainment. Secondly, this abnormal entrainment is studied by measuring PAC in the EEG

signals. PAC has become very prevalent in the analysis of time-series data from the brain (EEG and MEG). Although the PAC has been widely used, existing methods have some limitations such as limited frequency resolution and sensitivity to noise and data length. We use the modulation index (MI) defined by Tort et al. [35], which is considered one of the best performing methods. Thirdly, the PAC is the basis for the exploratory analysis of developmental dyslexia carried out by complex network analysis. As aforementioned, complex network analysis is playing an increasingly important role in the study of brain's structural and functional systems [1]. Here, we introduce the use of EEG frequency band coupling to create the graphs. This way of constructing the graphs has never been used to study DD, to the best of our knowledge. Thus, the PAC coupling information is treated as a graph in which the different nodes are the EEG bands (Delta, Theta, Alpha, Beta, Gamma) and the edges correspond to the PAC coupling between frequency bands.

The rest of this paper is developed as follows. In Section 2, database and methods used are described. Then, Sections 3 and 4 state and discuss the results of PAC analysis, complex network analysis and classification. Lastly, main conclusions and future works are given in Section 5.

2. Materials and methods

In this work, graph analysis is the principal tool to study the temporal evolution of the DD complex systems. This analysis is based on the EEG data obtained by the Leeduca research group at the University of Málaga [36]. Forty-eight participants took part in the study by the Leeduca Study Group. These subjects were matched in age ($t(1) = -1.4$, $p > 0.05$, age range: 88–100 months). The participants were 32 skilled readers of which 17 were males and 16 dyslexic readers (7 males). The control group had a mean age of 94.1 ± 3.3 months, and the dyslexic group 95.6 ± 2.9 months. The experiment was conducted in the presence of each child's legal guardians and with their understanding and written consent.

EEG signals were recorded using the Brainvision actiCHamp Plus with actiCAP (Brain Products GmbH, Germany). It had 32 active electrodes and was set at a sampling rate of 500 Hz. These electrodes were located in the 10–20 standardized system. Participants underwent 15-minute sessions in which they were presented white noise auditory stimuli modulated at 4.8, 16, and 40 Hz sequentially in ascending and descending order, for 2.5 min each. Participants were right-handed, native Spanish speakers. They had normal or corrected-to-normal vision and no hearing impairments. All dyslexic children in this study had received a formal diagnosis of dyslexia at school. None of the skilled readers reported having reading or spelling difficulties or have received a prior formal diagnosis of dyslexia.

2.1. Signal preprocessing

EEG signal preprocessing constitutes an important stage, due to the low signal-to-noise ratio of EEG signals and the number of artifacts presents in the signals. The preprocessing stage includes the following steps: first, artifacts corresponding to eye blinking were removed using blind source separation with Independent Component Analysis (ICA). The signal from each channel was independently normalized to zero mean and unit variance. Then it was referenced to the Cz electrode. Baseline correction was also applied. Finally, 15.02 s long windows were defined to segment the processed signals. The segmentation is done to correctly analyze the PAC temporal patterns [37]. We have chosen this window length as it is the optimum for our dataset. Thus, a sufficient number of slow oscillation cycles are taken into the

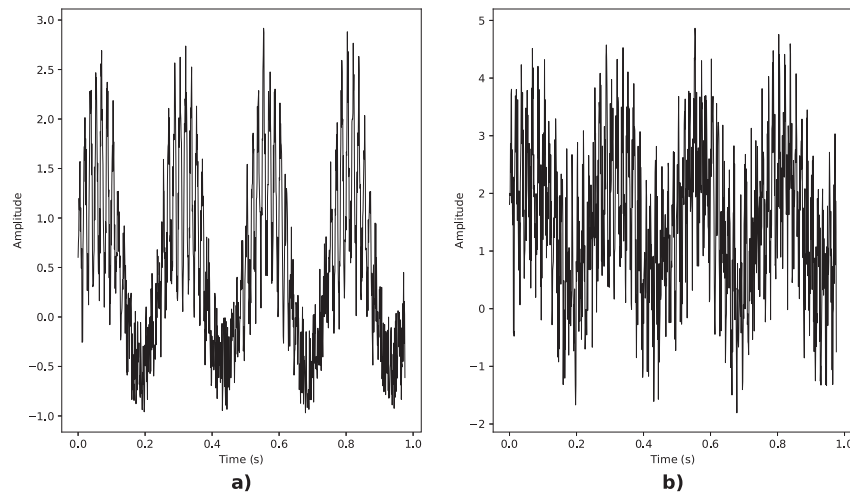


Fig. 1. Synthetic signals containing PAC between the phase of the band Theta (4 Hz) and the amplitude of the band Gamma (60 Hz). (a) Strong coupling. (b) Weak and noisy coupling.

temporal segment. Shorter windows result in overestimation of coupling and lower significance. According to [37], the length of the temporal segment is one of the most important requirements for robust PAC estimation. Moreover, it is a key concept for the statistical validation of the results by employing surrogate tests [37].

2.2. Phase–amplitude coupling

The representation of a complex system as a network requires the definitions of the nodes and edges that form the graphs. In this work, the edges correspond to the PAC measured between a pair of frequency bands. It is a key concept to understand the mechanism of coordination in neural dynamics across spatial and temporal scales [38]. According to Canolty et al. [39] Cross-Frequency Coupling (CFC) have a functional role representing the interaction between different brain rhythms. This forms a complex structure where information transfer occurs from large scale brain networks (where low-frequency brain rhythms are dynamically entrained) to local cortical processing reflected by high-frequency brain activity. CFC is potentially essential for understanding healthy and pathological brain function and the diagnosis of neural disorders [38]. The Phase–Amplitude CFC is a neural mechanism to study brain functions, that has received significant attention revealing its potential and limitations [37,40]. It is considered to have an important functional role [39]. The PAC CFC builds a framework for neural computation by regulating the frequency coupling in local and between different brain areas communication in large-scale brain networks [39]. This type of CFC is defined as the modulation of the amplitude of the high frequency oscillation by the phase of the low frequency component. Fig. 1 represents an example of two synthetic signals that contain PAC between the phase of the Theta band (4 Hz) and the amplitude of the Gamma band (60 Hz). The signal on the right shows a weaker and noisier coupling.

As we mentioned above, we measured the PAC as the coupling between the phase of a slow signal and the amplitude of a fast signal. In particular, the coupling between Delta, Theta, and Alpha (0.5–4, 4–8 and 8–12 Hz respectively) frequency bands providing the phase and Gamma (30–100 Hz) and Beta (12–30 Hz) frequency bands providing the amplitude. The phase of the Beta band is also included for measuring the coupling with the amplitude of the Gamma band. There are different PAC descriptors as presented in [41]: Phase-Locking Value, Mean Vector Length

(MVL), Modulation Index (MI), and Generalized-Linear-Modeling-Cross-Frequency-Coupling. In this way, there is still no agreement on how to calculate the PAC. Here, the modulation index (MI) is used, as defined by Tort et al. [35,42]. It is considered in [35] as one of the best performance methods for assessing the intensity of the PAC and it is well suited for the characteristics and length of the data used in the present work.

In order to calculate MI [35], it is necessary to extract the “phase-modulating” frequency band, f_p and the “amplitude-modulated” frequency band, f_A , from the raw signal, $x_{raw}(t)$. After filtering $x_{raw}(t)$ at the frequency ranges of f_p and f_A , the resulting signals are denoted as $x_{f_p}(t)$ and $x_{f_A}(t)$ respectively. Then, the time series of the phases of $x_{f_p}(t)$ and the time series of the amplitude envelope of $x_{f_A}(t)$ are obtained, named as $\Phi_{f_p}(t)$ and $A_{f_A}(t)$. Afterwards, all the phases $\Phi_{f_p}(t)$ are binned into eighteen 20 degrees intervals. The mean of $A_{f_A}(t)$ over each phase bin is computed as

$$P(j) = \frac{\bar{a}(j)}{\sum_{k=1}^N \bar{a}(k)} \tag{1}$$

where $\bar{a}(j)$ is the mean $A_{f_A}(t)$ value of the j phase bin. $N = 18$ is the total number of bins, and P is referred to as the “amplitude distribution”. Fig. 2 shows the amplitude distribution over phase bins from the synthetic signals of Fig. 1. It is important to note that this amplitude distribution is not normalized as the defined mean amplitude distribution, but represents the same characteristic information.

If there is no phase–amplitude coupling, the amplitude distribution P over the phase bins is uniform. Thus, the existence of PAC is characterized by a deviation of the amplitude distribution P from the uniform distribution, U . Tort et al. [35] defined the MI as an adaptation of the Kullback–Leibler (KL) divergence [43] as

$$KL(P, Q) = \sum_{j=1}^N P(j) \log \frac{P(j)}{Q(j)} \tag{2}$$

It is a widely used metric in statistics and in information theory to measure how one probability distribution is different from another probability distribution Q . The distribution divergence measure is made to assume values between 0 and 1. It is useful to notice that the Shannon entropy $H(p)$ is defined as

$$H(P) = - \sum_{j=1}^N P(j) \log P(j) \tag{3}$$

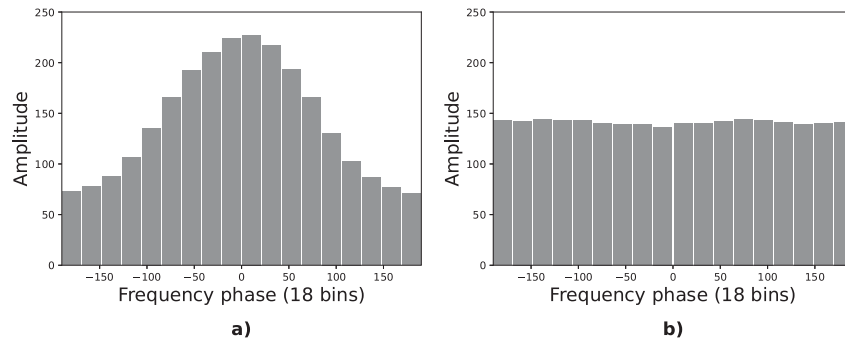


Fig. 2. Amplitude distribution over phase bins. (a) Theta phase. (b) Alpha phase. The synthetic signal contains PAC where the phase of the Theta band modulates the amplitude of the Gamma band. Thus, (a) shows an amplitude distribution that corresponds to the presence of PAC.

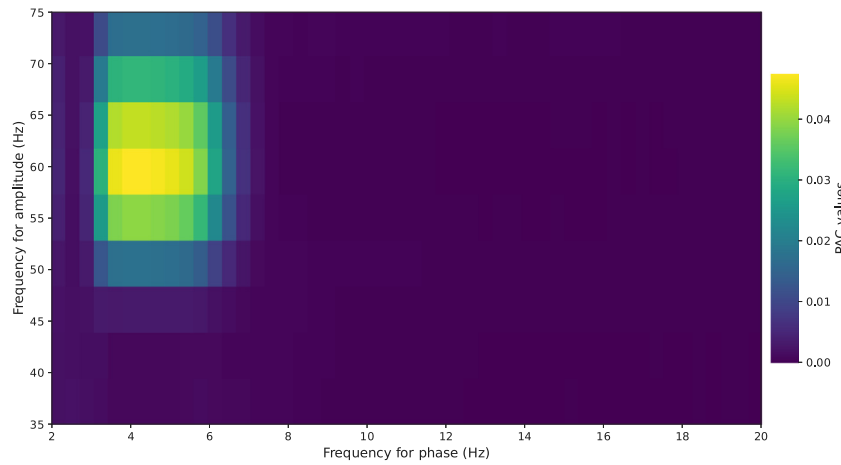


Fig. 3. Phase-amplitude comodulogram showing a coupling between Theta and Gamma bands.

It represents the amount of information inherent in a variable. If it is maximal, all the phase bins have the same amplitude (uniform distribution). In this adaptation of the KL divergence, the relation to the Shannon entropy is described as

$$KL(P, U) = \log N - H(P) \tag{4}$$

where P is the defined amplitude distribution and U is the uniform distribution. Finally, the MI is calculated by the below formula:

$$MI = \frac{KL(P, U)}{\log N} \tag{5}$$

The MI results were analyzed using surrogate time series obtained from the creation of shuffled versions of $\Phi_{f_p}(t)$ and $A_{f_A}(t)$ time series. Then, this shuffled series are used to estimate a surrogate MI and this procedure is repeated several hundred times. The distribution thus obtained is considered an approximation of the null distribution [44] and allows us to test the significance of the MI values. This null distribution enables us to infer whether the observed value actually differs from what would be expected from chance [35]. To this end, 200 surrogate MI values are generated to assess the significance of the results, considering $p < 0.05$ as significant. Additionally, the MI measure is represented in a phase-amplitude comodulogram. This is a tool to represent the coupling measured among multiple frequency bands, and it is ideal to explore the PAC [35]. The MI calculated for the synthetic PAC signal is shown in Fig. 3 where the phase of the Theta band (f_p) modulates the amplitude of the Gamma band (f_A).

To sum up, PAC is measured by MI in each temporal segment for every electrode. This allows to explore the temporal evolution

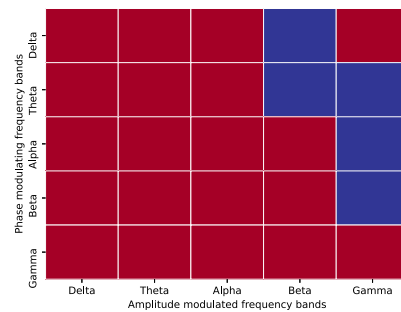


Fig. 4. Adjacency matrix from Table 1. Blue indicates coupling and red indicates no coupling.

of each subject's response to auditory stimuli. Thus, the PAC MI values are used to construct the nodes and edges of the coupling networks between frequency bands. We used the open-source Python toolbox, Tensorpac [45], to compute the PAC. It is focused on PAC analysis of neurophysiological data.

2.3. Complex network analysis

Complex networks are all around us and are present in many scientific and technological areas, describing a wide range of real systems in nature and society. The principal tool to study these complex systems is graph theory [46]. As a natural framework for the treatment of complex networks, it is useful to describe some common properties and how they are measured. A complex network is represented as a graph $G(N, K)$, that is, two sets of N

nodes and K links or edges. The graphs are undirected or directed and weighted or unweighted. In an undirected graph, each of the links is defined by a couple of nodes i and j , and is denoted as (i, j) . In a directed graph, the order of the two nodes is important: (i, j) stands for a link from i to j and (j, i) is a different link from j to i . An unweighted graph has a binary nature, i.e. the edges are present or not. In contrast, in a weighted graph each edge is a measure of the strength of the connection [46]. If there are loops or multiple edges, they are called multigraphs. A graph is completely described by its adjacency matrix, A . It is a $N \times N$ matrix where a_{ij} with $(i, j = 1, 2, \dots, N)$ is equal to 1 when the edge l_{ij} exists, and zero otherwise. In this work, the adjacency matrix (Fig. 4) is a 5×5 asymmetric matrix from the frequency bands considered as nodes. The entry a_{ij} is one if there is significant PAC measured in at least an electrode between two frequency bands. This is shown in Table 1.

The node degree, which is one of the most important descriptors for complex networks, is computed as:

$$k_i = \sum_{j=1}^N a_{ij} \quad (6)$$

where k_i is the degree of a node i and a_{ij} is an entry for the adjacency matrix. This way, considering the number of connections that link it to the rest of the network. The degree distribution is drawn from the degree of all nodes. Another measure directly related to the node degree is the assortativity. It is “the correlation between the degrees of connected nodes” [1]. Furthermore, the relation between the actual number of edges and the number of possible edges of a graph provide the density as

$$D = \frac{K}{N(N-1)} \quad (7)$$

for directed graphs.

The clustering coefficient C is defined as follows [47]. Suppose that a node i has k_i neighbors. In this situation, the number of edges that exist between them are $k_i(k_i - 1)/2$ at most (in the case that every neighbor of i is connected to each other). Let C_i denote the edges that actually exist from all the possible. C is defined as the average of C_i over all i .

$$C = \frac{1}{N} \sum_{i=1}^N C_i \quad (8)$$

where N is the total number of vertices and C_i is the clustering coefficient of vertex i .

Path length, L , is defined in [47] as the number of edges that form the shortest path between two vertices. This measure is averaged over all pairs of vertices

$$L = \frac{1}{N} \sum_{i=1}^N L_i \quad (9)$$

where L_i is the average distance between vertex i and all other vertex.

The centrality, in general terms, quantifies the relative relevance of a given node in a network. The node betweenness measures how many of the shortest paths between all other node pairs in the network pass through a node. The node closeness is the inverse of the sum of the path length from all other nodes [46]. The degree, closeness and betweenness are the standard measures of node centrality.

The study of real networks has shown the existence of bridging links that connect different areas of most of the networks. This means that there is a short path between any two nodes that speed up the communication among nodes [46]. This particular organization is known as the small-world property or

small-worldness. Networks with such topology are named small-world networks and are typified by having a small value of L , like random graphs, and a high clustering coefficient C , like regular lattices than would be expected by chance [47,48]. The small-worldness of a network is measured by comparing it to an Erdős-Rényi (E-R) [49] random graph with the same nodes and edges. For this purpose, a quantitative metric of small-worldness, S , is defined as

$$S = \frac{\gamma}{\delta} = \frac{\frac{C}{C_{rand}}}{\frac{L}{L_{rand}}} \quad (10)$$

where L is the mean shortest path length of a network and C its clustering coefficient. L_{rand} and C_{rand} are the respective quantities for the corresponding E-R random graph. From [50] a network is said to be a small-world network if $L \geq L_{rand}$ and $C \gg C_{rand}$. Thus, a network is said to be a small-world network if $S > 1$.

2.3.1. Network construction

There are numerous works [51–53] about the study of characteristics of complex networks. It is defined as a network with certain topological features such as high clustering, small-worldness, the presence of high-degree nodes or hubs, assortativity, modularity or hierarchy. This does not occur or are not typical of simple networks such as random graphs or regular lattices [1]. The complex network used in this work are based in the MI explained in the above section. In this way, we employed directed and unweighted graphs with the nodes being the typical EEG frequency bands. Thus, the edges of the graphs correspond to the presence of significant PAC in at least an electrode between a pair of frequency bands. In the case that there is more than one electrode with PAC, we select the highest PAC value to represent the coupling between the two bands. The edges have a direction from a band providing the phase to another band whose amplitude is modulated. These edges are binarized, therefore, unweighted. From the adjacency matrix in Table 1, the graph shown in Fig. 5 is obtained. Each entry of the adjacency matrix equal to 1 is due to a significant PAC MI value in an electrode for a determined combination of frequency bands. This is represented on the left part of Fig. 5. Then, graphs are obtained for each subject and each temporal segment, enabling the study of the network characteristics through time. This has been done with the use of the Python package NetworkX that is meant for the creation, manipulation, and study of the structure, dynamics, and functions of complex networks [54].

3. Experimental results

We present the results for the PAC analysis, complex network analysis and classification. First, we start with the results of the PAC analysis over the temporal segments that allow the exploratory analysis. To this end, the MI measured intra-electrode is represented for each frequency band combination considered. With this, extracting information about the temporal evolution of the PAC for dyslexic and control subjects. Then, we focus on the complex network analysis, obtaining metrics to study the networks and the evolution of their characteristics through time. Finally, these metrics are used as features to train a SVM classifier to perform a classification test.

3.1. PAC results

The PAC is measured and presented as a function of temporal segments. A set of frequency band pairs are defined in Tensorpac

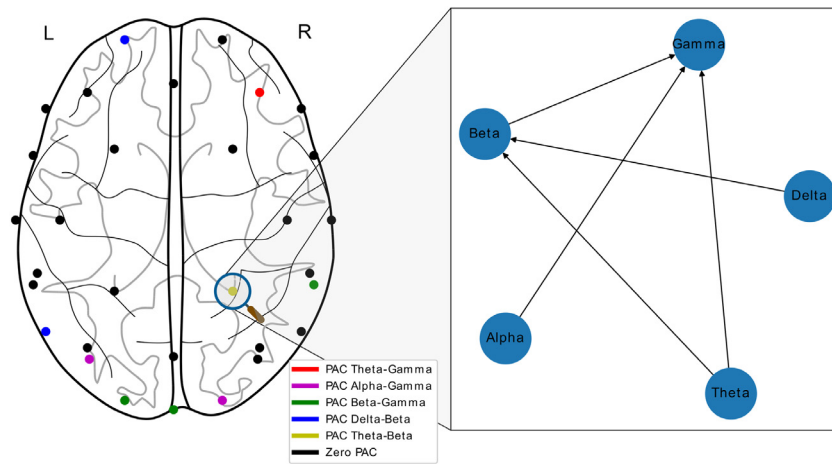


Fig. 5. Frequency bands source for PAC and graph from adjacency matrix in Table 1.

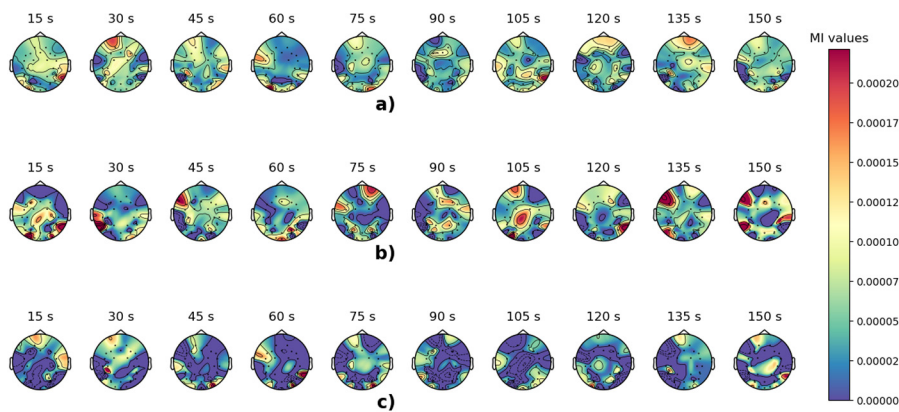


Fig. 6. Average MI topoplots for Theta and Beta frequency bands and 4.8 Hz stimulus. (a) Controls. (b) Dyslexics. (c) Controls and dyslexics difference.

to study and identify a temporal behavior by measuring the MI. These combinations of frequency bands are: Delta-Gamma, Theta-Gamma, Alpha-Gamma, Beta-Gamma, Delta-Beta, Theta-Beta and Alpha-Beta. The PAC is obtained by measuring the MI in each electrode for all these combinations and for each subject and each temporal segment. These MIs are represented in topoplots of the average PAC measured. Thus, information about changes in the temporal response to the stimulus is drawn for dyslexic and control subjects at each combination of frequencies. Fig. 6 shows the average MI measured for each segment and every subject between the Theta and Beta frequency bands. In Fig. 6(a) and (b) the MI for controls and dyslexics are presented, respectively. The differences in the temporal evolution is easier to see and interpret in Fig. 6(c). This set of topoplots represents the differences in the average MI value between dyslexics and controls. The topoplots in Fig. 7 shows the difference between controls and dyslexics for the MI measured in the rest of frequency bands combinations.

3.2. Complex network analysis results

In this section, the selected characteristics of the complex networks that have been measured are presented. From the MI results of the PAC analysis, a set of ten graphs (one for each temporal segment) have been created for each subject. To clarify, each graph contains the information of the measured MI of all electrodes for a temporal segment of one subject. Thus, as we can see in Fig. 8 the edges in the graph represents the existence of measured PAC in an electrode. These edges appear from a node

indicating the “phase modulating” frequency band, to the pointed node representing the “amplitude modulated” frequency band.

The number of edges of the graphs varies between subjects and temporal segments. This is shown in Fig. 9, where for certain temporal segments the number of edges differ from dyslexic to control subjects.

Once the graphs are calculated, we measured the selected metrics. First, the segregation of the networks is characterized with the clustering coefficient. Second, the characteristic path length is measured obtaining the average path length of each graph. These metrics make possible to calculate the small-worldness of the complex networks for each subject and segment. This is shown in Fig. 10 where the graphs have a small-world topology ($S > 1$). Finding more differences in the small-worldness between groups for the 4.8 Hz stimulus.

3.3. Classification

Here, the metrics obtained from the analysis of the characteristics of complex networks are used as features to train a SVM [55] classifier. In particular, the classification results from the small-worldness property are presented and discussed as it achieves a better performance. Using the small-worldness data, a $N \times M$ matrix has been created with N , the number of subjects, and M , the number of segments in which the small-worldness is measured. The accuracy, sensitivity and specificity are the metrics used to assess the classification performance. We also obtain the Area Under ROC Curve (AUC) for each case. Then, cross validation is applied to the data using a K-fold stratified scheme with 5 folds.

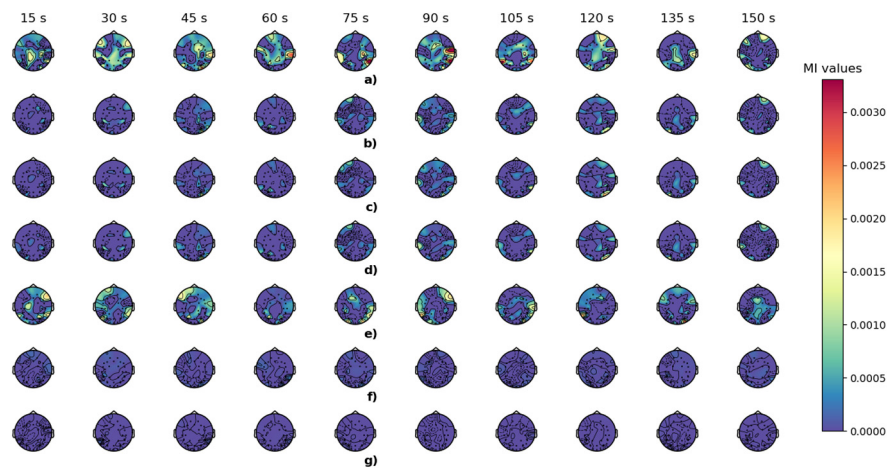


Fig. 7. Average difference MI topoplots for 4.8 Hz. (a) Delta-Gamma bands. (b) Theta-Gamma bands. (c) Alpha-Gamma bands. (d) Beta-Gamma bands. (e) Delta-Beta bands. (f) Theta-Beta bands. (g) Alpha-Beta bands.

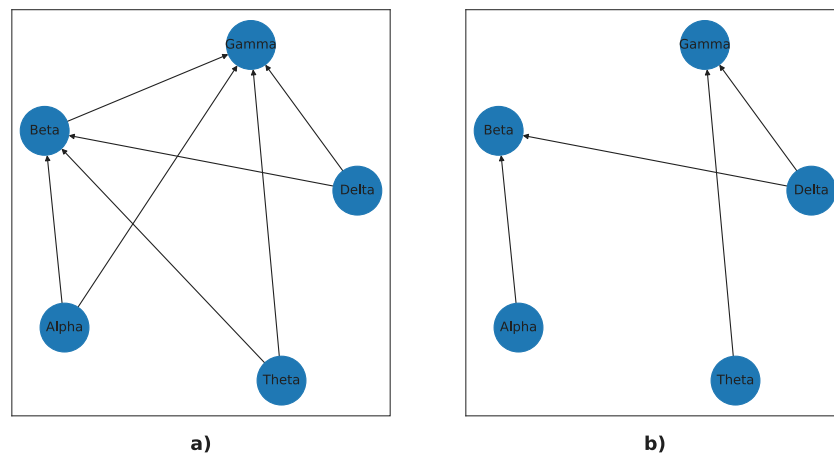


Fig. 8. Graphs showing the presence of MI intra-electrode PAC in a pair of EEG bands. (a) Control subjects. (b) Dyslexic subjects.

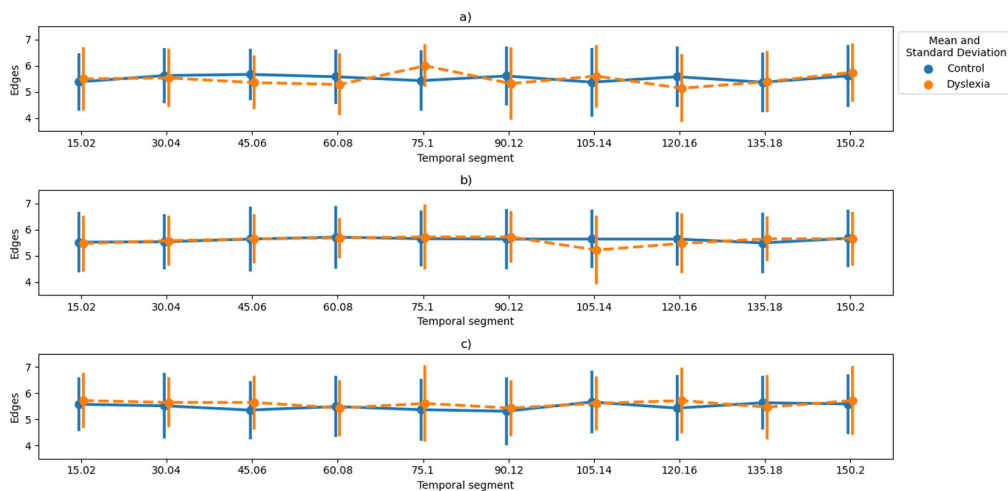


Fig. 9. Number of edges for dyslexic and control subjects and each temporal segment. (a) 4.8 Hz. (b) 16 Hz (c) 40 Hz.

As it is exposed in the above section, the graphs obtained for the 4.8 Hz stimulus PAC measured implied a greater difference in the small-worldness between groups. This results in a better classification performance for 4.8 Hz stimulus using the small-worldness data that is shown in Fig. 11. In this figure the accuracy,

sensitivity, specificity and AUC are represented. Metrics for other features are shown in Table 2.

At this point, it is important to estimate the significance of the classification accuracy obtained and evaluate whether the classifier has found a real connection between the data and the

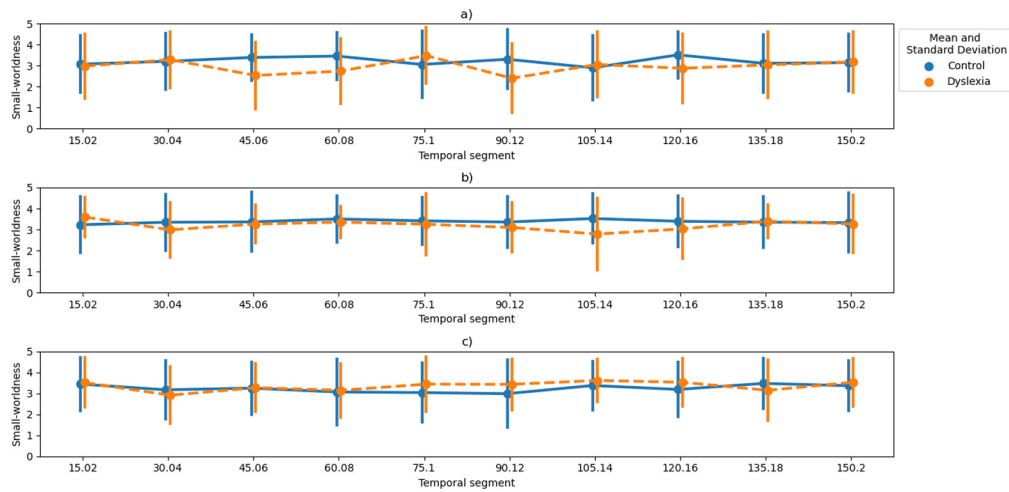


Fig. 10. Average small-worldness. (a) 4.8 Hz. (b) 16 Hz. (c) 40 Hz.

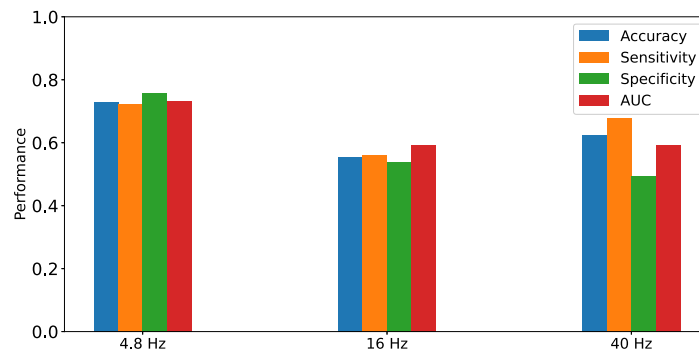


Fig. 11. Classification results for 4.8 Hz, 16 Hz and 40 Hz.

Table 1 Example of adjacency matrix for a dyslexic subject.

	Delta	Theta	Alpha	Beta	Gamma
Delta	0	0	0	1	0
Theta	0	0	0	1	1
Alpha	0	0	0	0	1
Beta	0	0	0	0	1
Gamma	0	0	0	0	0

class labels [56]. Permutation tests are used for this purpose, providing useful statistics about the underlying reasons for the obtained classification result. Thus, under the null hypothesis that the features and the labels are independent the null distribution is estimated by 1000 permutations of the dataset labels in a 5-fold cross validation scheme. The p-values obtained represent the fraction of random datasets where the classifier behaved as well as or better than in the original data. Fig. 12 illustrates the accuracy obtained by the random data and the original score along with the corresponding p-value for each case. The p-value is only lower than 0.05 for the 4.8 Hz data. Consequently, a significant accuracy score is obtained and is greater than for the random data.

4. Discussion

The application of graph theory to complex networks is a promising area to study the brain and its pathologies. In the present work, we have performed an exploratory analysis using complex networks that are extracted from PAC. This PAC has been

measured between the typical EEG frequency bands: Delta, Theta, Alpha, Beta and Gamma. All the effort is oriented to advance towards an early Developmental Dyslexia diagnosis and a better understanding of its neural basis. There are other works that have studied this neurological disorder to develop machine learning methods for detecting Dyslexia as in Table 3 using EEG, fMRI and MRI. For this, it is fundamental to count with a database that offer adequate EEG data from control and dyslexics subjects. In this case, the Leeduca Study Group provided the database. It is obtained from the experiment where a set of three auditory stimulus 4.8, 16 and 40 Hz is presented to controls and dyslexics. According to Goswami [57] this auditory stimulus are related to the oscillatory phase entrainment to speech in brain that are thought to be important for speech encoding. Furthermore, it is reinforced in [34] the existence of phonological impairments in all linguistic levels in dyslexics children such as stressed syllables, syllables, onset-rimes, and phonemes. The last decade has faced a change of the approach to language processing with new tools and ideas. This was stated in Poeppel [58], where it is pointed out that the system for speech and language processing is considerably more complex and distributed.

Neural oscillations have become a promising mechanism for studying the processes of learning and language. The MI as defined by Tort et al. [35] has been used to obtain the PAC intra-electrode for each subject and for every temporal segment specified. The PAC results are shown in topoplots that represents the electrode activation in terms of the MI values. The results for the Theta-Beta PAC in the 4.8 Hz stimulus are presented in Fig. 6 as an example of the outcome of the PAC analysis. This figure shows the evolution of the average MI for both control

Table 2
Classification comparative using graph metrics as SVM features.

Stimulus	Features	Accuracy	Sensitivity	Specificity	AUC
4.8 Hz	Small-Worldness	0.729	0.723	0.747	0.733
	Average Degree	0.519	0.467	0.647	0.575
	Assortativity	0.489	0.4	0.71	0.626
	Density	0.372	0.23	0.727	0.518
	Betweenness Centrality	0.522	0.458	0.6	0.595
	Best two-features combination: Small-Worldness and Average Degree	0.726	0.716	0.753	0.739
	Best three-features combination: Small-Worldness, Average Degree and Betweenness Centrality	0.516	0.6	0.4	0.753
	Best four-features combination: Small-Worldness, Average Degree, Density and Betweenness Centrality	0.516	0.6	0.4	0.75
	16 Hz	Small-Worldness	0.554	0.5612	0.54
Degree		0.438	0.445	0.433	0.426
Assortativity		0.511	0.354	0.893	0.629
Density		0.573	0.632	0.433	0.524
Betweenness Centrality		0.372	0.2	0.8	0.659
Best two-features combination: Small-Worldness and Average Degree		0.522	0.519	0.54	0.622
Best three-features combination: Small-Worldness, Average Degree and Density		0.49	0.34	0.86	0.622
Best four-features combination: Small-Worldness, Assortativity, Density and Betweenness Centrality		0.372	0.2	0.8	0.632
40 Hz		Small-Worldness	0.624	0.678	0.493
	Degree	0.5	0.512	0.473	0.53
	Assortativity	0.371	0.2	0.8	0.626
	Density	0.564	0.559	0.573	0.596
	Betweenness Centrality	0.372	0.2	0.8	0.555
	Best two-features combination: Small-Worldness and Average Degree	0.509	0.455	0.647	0.616
	Best three-features combination: Small-Worldness, Average Degree and Density	0.635	0.765	0.32	0.627
	Best four-features combination: Small-Worldness, Assortativity, Density and Betweenness Centrality	0.372	0.2	0.8	0.622

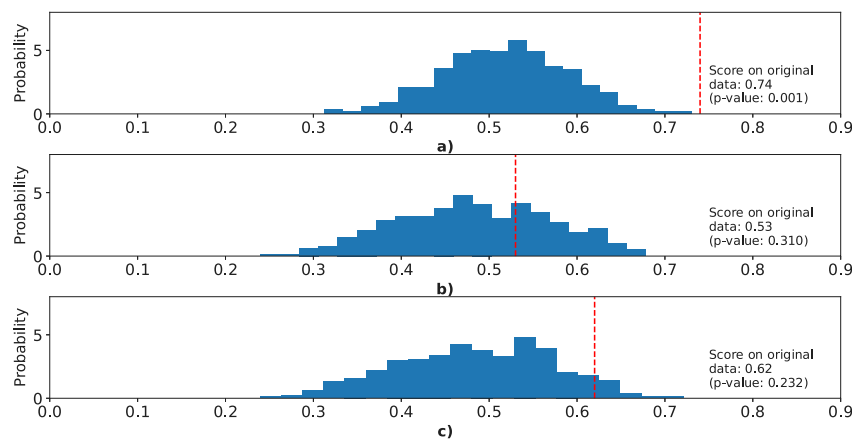


Fig. 12. Results of the permutation tests using the small-worldness property as a feature. (a) 4.8 Hz. (b) 16 Hz. (c) 40 Hz.

and dyslexic groups (Fig. 6(a) and Fig. 6(b), respectively) through each temporal segment and in every electrode. To visualize the distinction between groups, it is represented the difference of the mean MI as in Fig. 6(c). There is a high variability in the topoplots of each subject, and that makes it difficult to perform a visual analysis of the differences. To overcome this, the difference average MI for each frequency band combinations is represented in Fig. 7 for the 4.8 Hz stimulus, showing larger differences for the temporal segments of the PAC from Delta-Gamma and Delta-Beta. This implies that for these bands the response to the auditory stimulus differ over time for controls and dyslexics.

A set of complex networks have been created from the PAC measured. These networks represent the interaction between frequency bands through time by means of intra-electrode PAC. An example of this is shown in Fig. 8. Each graph shows the results of PAC between every pair of frequency bands for each subject and each temporal segment, highlighting the presence of PAC in one or several electrodes. Among all the subjects the

graphs obtained differ in the number of edges for certain temporal segments as it is shown in Fig. 9. This suggests that the number of electrodes with significant PAC measured varies over time with the evolution of the response to the auditory stimulus. Then, the graph metrics are calculated to study the characteristics and its evolution through time. From all the results the property of small worldness is highlighted (Fig. 10), denoting a small-world topology in agreement with other brain complex networks as stated in [16]. Works as [1,16] provide strong evidence that brain networks exhibit small-world attributes and this is preserved across multiple frequency bands. From these results, it is noted that there are larger differences in the small-worldness for the 4.8 Hz stimulus across temporal segments. According to the Temporal Sampling Framework (TSF) [57] the neural oscillations in auditory cortex encode the acoustic speech signal. It is proposed that the phonological deficit in DD emerges from an atypical neural entrainment to the slower amplitude modulations present in the speech signal (below 10 Hz) [30]. Thus, the differences

Table 3
Classification results obtained in different works using structural imaging (MRI), functional imaging (fMRI) and electroencephalography (EEG).

Author	Sample size	Acquisition technique	Number of electrodes	Stimulus	Machine learning method	Classifier performance
Cui et al. [59]	61	MRI	-	Reading	SVM	Acc=0.836± ^a Sens=0.75± ^a Spec=0.909± ^a AUC=0.86± ^a
Łłoński et al. [60]	236	MRI	-	Reading	SVM LR RF	Acc=0.65± ^a Sens= ^a Spec= ^a AUC=0.66± ^a
Frid and Manevitz [61]	32	EEG	64	Reading	SVM	Confusion matrix
Perera et al. [62]	32	EEG	32	Typing and writing	SVM	Acc=0.718± ^a Sens=0.764± ^a Spec=0.667± ^a AUC=0.86± ^a
Rezvani et al. [63]	44	EEG	64	Typing and writing	SVM	Acc=0.953± ^a Sens=0.964± ^a Spec=0.933± ^a AUC= ^a
Frid and Breznitz [64]	50	EEG	64	Auditory	SVM	Acc=0.85 ± 0.1 Sens=0.749 ± 0.2 Spec=0.822 ± 0.12 AUC= ^a
Chimeno et al. [65]	56	fMRI	32	Tests	ANN	Acc=0.949± ^a Sens=0.947± ^a Spec=0.95± ^a AUC= ^a
Zahia et al. [66]	66	fMRI	32	Reading	3D CNN	Acc=0.727± ^a Sens=0.75± ^a Spec=0.714± ^a AUC= ^a
Ortiz et al. [67]	48	EEG	32	Auditory	SVM	Acc=0.78± ^a Sens=0.66± ^a Spec=0.81± ^a AUC=0.83± ^a
Martinez-Murcia et al. [68]	48	EEG	32	Auditory	Autoencoder	Acc=0.74 ± 0.114 Sens=0.596 ± 0.254 Spec=0.79 ± 0.221 AUC=0.762± ^a
Martinez-Murcia et al. [69]	48	EEG	32	Auditory	SVM	Acc=0.728± ^a Sens=0.667± ^a Spec=0.789± ^a AUC=0.748± ^a

^aData not available in the source.

found for the 4.8 Hz stimulus are consistent with the TSF. These differences can be generated by a more complex auditory processing in dyslexics, attempting to overcome the poorly encoding of prosodic and syllabic information.

In Table 2 the classification results for all the metrics studied in this work are presented. From this, we assess the classification performance of every metric and concluded that the small-worldness property has a larger discrimination capacity. We also show the best classification results for the two-, three- and four-feature combinations. The combination of small-worldness and average degree achieved similar results to those obtained with the exclusive use of small-worldness for 4.8 Hz and 16 Hz stimuli. The best classification results are for the 4.8 Hz stimulus with the small-worldness property achieving an accuracy of 0.729, 0.723 sensitivity, 0.747 specificity and an AUC of 0.733, as shown in

Fig. 11. For all stimuli, the small-world property provide with better classification results than other metrics. Then, a permutation test is performed to estimate the significance of the classification accuracy obtained. Fig. 12 indicates that the *p*-value is only lower than 0.05 for the 4.8 Hz small-worldness data, thus rejecting the null hypothesis and finding a real connection between the data and the class labels.

Finally, a potential limitation of this study is the relatively small sample size of the dataset. This is commonplace in studies involving children with dyslexia, due to difficulties in recruiting experimental subjects. This contextual information is also key to compare these results to other studies, and therefore, the sample size for each study has been added to Table 3 to assist in the interpretation.

5. Conclusions

The small-world attributes are present in the majority of functional brain networks. This has been the starting point of this work, the concept that network organization in neurological disease reflects a deviation from the optimal pattern. Even though the complex networks studied in this work are not directly functional brain networks, they are obtained from PAC brain coupling for each electrode under an experimental setup using non-interactive and non-speech auditory stimuli. This corresponds to the sampling processes developed in the brain during language processing and consists of bandwidth-limited white noise modulated in amplitude with 4.8, 16 and 40-Hz signals. Moreover, the networks provide information related to the frequency bands and temporal evolution of the PAC in the electrodes.

Graph theoretical analysis reveals abnormal patterns of organization that correspond to neurological disorders. The complex networks studied present small-world characteristics as having a high clustering coefficient and a small value of path length. However, the graphs have different pattern topology over time for control and dyslexic subjects. This underlines a increased complexity of auditory processing in dyslexics, as they attempt to employ different neural mechanisms to overcome the phonological deficit. After graph analysis, these metrics were used as SVM features in order to classify the subjects. As a result, the small-world property provides discriminant information to achieve AUC values up to 0.733, and obtaining the best accuracy for the 4.8 Hz stimulus.

It is worth noting that the main aim of this work was to provide a methodology for the exploratory analysis of the brain processes involved in low-level auditory processing, analyzed from a coupling point of view and modeled by complex network analysis. However, the results obtained show that complex network based features are able to differentiate between controls and dyslexic subjects with similar sensitivity and specificity values than other discriminative methods (Table 3). In future works, we plan to extend the current study by combining it with functional brain networks. This should help to achieve better results relevant to the diagnosis and early detection of DD. This is performed by measuring PAC inter-electrode, obtaining complex networks, where it is more direct to extract information about the underlying neurocognitive profiles in DD. Another possible way is to improve the extraction of the phase and amplitude time series with the use of adaptive decomposition methods as Empirical Mode Decomposition (EMD).

CRedit authorship contribution statement

Nicolás J. Gallego-Molina: Conceptualization, Methodology, Software, Data curation, Writing – original draft, Visualization, Investigation, Validation. **Andrés Ortiz:** Conceptualization, Methodology, Software, Supervision, Software, Validation, Writing – reviewing and editing. **Francisco J. Martínez-Murcia:** Methodology, Software, Visualization, Investigation, Supervision, Writing – reviewing and editing. **Marco A. Formoso:** Data curation, Software, Validation. **Almudena Giménez:** Software, Validation, Writing – reviewing and editing.

Declaration of competing interest

The authors declare that they have no known competing financial interests or personal relationships that could have appeared to influence the work reported in this paper.

Acknowledgments

This work was supported by projects PGC2018-098813-B-C32 (Spanish “Ministerio de Ciencia, Innovación y Universidades”), UMA20-FEDERJA-086 (Consejería de economía y conocimiento, Junta de Andalucía) and by European Regional Development Funds (ERDF). We gratefully acknowledge the support of NVIDIA Corporation with the donation of one of the GPUs used for this research. Work by F.J.M.M. was supported by the MICINN “Juan de la Cierva - Incorporación” Fellowship. We also thank the *Leeduca* research group and Junta de Andalucía for the data supplied and the support. Funding for open access charge: Universidad de Málaga/CBUA.

References

- [1] E. Bullmore, O. Sporns, Complex brain networks: Graph theoretical analysis of structural and functional systems, *Nat. Rev. Neurosci.* 10 (3) (2009) 186–198.
- [2] M. Rubinov, O. Sporns, Complex network measures of brain connectivity: uses and interpretations, *Computational Models of the Brain, NeuroImage* 52 (3) (2010) 1059–1069.
- [3] C. Stam, B. Jones, G. Nolte, M. Breakspear, P. Scheltens, Small-world networks and functional connectivity in Alzheimer's disease, *Cerebral Cortex* 17 (1) (2006) 92–99.
- [4] F. Vecchio, F. Miraglia, C. Marra, D. Quaranta, M. Vita, P. Bramanti, P. Rossini, Human brain networks in cognitive decline: a graph theoretical analysis of cortical connectivity from EEG data, *J. Alzheimers Disease JAD* 41 (2014).
- [5] A. Ortiz, J. Munilla, I. Álvarez-Illán, J.M. Górriz, J. Ramírez, A.D.N. Initiative, Exploratory graphical models of functional and structural connectivity patterns for Alzheimer's disease diagnosis, *Front. Comput. Neurosci.* 9 (2015).
- [6] J. Munilla, A. Ortiz, J.M. Górriz, J. Ramírez, the Alzheimer's Disease Neuroimaging Initiative, Construction and analysis of weighted brain networks from SICE for the study of Alzheimer's disease, *Front. Neuroinformatics* 11 (2017).
- [7] E.P. Leitgeb, M. Šterk, T. Petrijan, P. Gradišnik, M. Gosak, The brain as a complex network: Assessment of EEG-based functional connectivity patterns in patients with childhood absence epilepsy, *Epileptic Disord.* 22 (5) (2020) 519–530.
- [8] L. Rutter, S.R. Nadar, T. Holroyd, F.W. Carver, J. Apud, D.R. Weinberger, R. Coppola, Graph theoretical analysis of resting magnetoencephalographic functional connectivity networks, *Front. Comput. Neurosci.* 7 (2013).
- [9] R.L. Peterson, B.F. Pennington, Developmental dyslexia, *Lancet* 379 (9830) (2012) 1997–2007.
- [10] C. Cortiella, S. Horowitz, *The State Of Learning Disabilities: Facts, Trends And Emerging Issues*, third ed., National Center for Learning Disabilities, 2014.
- [11] P.A. Thompson, C. Hulme, H.M. Nash, D. Gooch, E. Hayiou-Thomas, M.J. Snowling, Developmental Dyslexia: Predicting individual risk, *J. Child. Psychol. Psychiatry.* 56 (9) (2015) 976–987.
- [12] E.S. Finn, X. Shen, J.M. Holahan, D. Scheinost, C. Lacadie, X. Papademetris, S.E. Shaywitz, B.A. Shaywitz, R.T. Constable, Disruption of functional networks in Dyslexia: a whole-brain, data-driven analysis of connectivity, *Development of Social Cognition in Developmental Disorders, Biol. Psychiat.* 76 (5) (2014) 397–404.
- [13] E.S. Edwards, K. Burke, J.R. Booth, C. McNorgan, Dyslexia on a continuum: A complex network approach, in: S. Hayasaka (Ed.), *PLoS One* 13 (12) (2018) e0208923.
- [14] T. Qi, B. Gu, G. Ding, G. Gong, C. Lu, D. Peng, J.G. Malins, L. Liu, More bilateral, more anterior: Alterations of brain organization in the large-scale structural network in Chinese dyslexia, *NeuroImage* 124 (2016) 63–74.
- [15] S.K. Bailey, K.S. Aboud, T.Q. Nguyen, L.E. Cutting, Applying a network framework to the neurobiology of reading and dyslexia, *J. Neurodev. Disord.* 10 (1) (2018) 37.
- [16] O. Sporns, C.J. Honey, Small worlds inside big brains, *Proc. Natl. Acad. Sci.* 103 (51) (2006) 19219–19220.
- [17] P. An, Z. Yuan, J. Zhao, X. Jiang, B. Du, An effective multi-model fusion method for EEG-based sleep stage classification, *Knowl.-Based Syst.* 219 (2021) 106890.
- [18] H. Huang, J. Zhang, L. Zhu, J. Tang, G. Lin, W. Kong, X. Lei, L. Zhu, EEG-based sleep staging analysis with functional connectivity, *Sensors* 21 (6) (2021) 1988.
- [19] M. Sharma, V. Patel, U.R. Acharya, Automated identification of insomnia using optimal bi-orthogonal wavelet transform technique with single-channel EEG signals, *Knowl.-Based Syst.* 224 (2021) 107078.

- [20] F.-G. Tang, Y. Liu, Y. Li, Z.-W. Peng, A unified multi-level spectral-temporal feature learning framework for patient-specific seizure onset detection in EEG signals, *Knowl.-Based Syst.* 205 (2020) 106152.
- [21] N. Darjani, H. Omranpour, Phase space elliptic density feature for epileptic EEG signals classification using metaheuristic optimization method, *Knowl.-Based Syst.* 205 (2020) 106276.
- [22] G. Fraga González, M.J.W. Van der Molen, G. Žarić, M. Bonte, J. Tijms, L. Blomert, C.J. Stam, M.W. Van der Molen, Graph analysis of EEG resting state functional networks in dyslexic readers, *Clin. Neurophysiol.* 127 (9) (2016) 3165–3175.
- [23] K.F.H. Lui, J.C.M. Lo, C.S.-H. Ho, C. McBride, U. Maurer, Resting state EEG network modularity predicts literacy skills in L1 Chinese but not in L2 English, *Brain Lang.* 220 (2021) 104984.
- [24] T. Taskov, J. Dushanova, Reading multiple EEG frequency-band networks in developmental dyslexia, in: D. Russo, T. Ahram, W. Karwowski, G. Di Bucchianico, R. Tajar (Eds.), *Intelligent Human Systems Integration 2021*, in: *Advances in Intelligent Systems and Computing*, Springer International Publishing, Cham, 2021, pp. 171–180.
- [25] G. Fraga-González, D.J.A. Smit, M.J.W. Van der Molen, J. Tijms, C.J. Stam, E.J.C. de Geus, M.W. Van der Molen, Graph analysis of EEG functional connectivity networks during a letter-speech sound binding task in adult dyslexics, *Front. Psychol.* 12 (2021) 5344.
- [26] J. Dushanova, S. Tsokov, Altered electroencephalographic networks in developmental dyslexia after remedial training: A prospective case-control study, *Neural Regen. Res.* 16 (4) (2021) 734.
- [27] T. Taskov, J. Dushanova, Functional connectivity in developmental dyslexia during speed discrimination, *Symmetry* 13 (5) (2021) 749.
- [28] G. Žarić, J.a.M. Correia, G. Fraga González, J. Tijms, M.W. van der Molen, L. Blomert, M. Bonte, Altered patterns of directed connectivity within the reading network of dyslexic children and their relation to reading dysfluency, *Dev. Cogn. Neurosci.* 23 (2017) 1–13.
- [29] F.J. Martínez-Murcia, A. Ortiz, J.M. Gorriç, J. Ramirez, P.J. Lopez-Abarejo, M. Lopez-Zamora, J.L. Luque, EEG connectivity analysis using denoising autoencoders for the detection of dyslexia, *Int. J. Neural Syst.* 30 (07) (2020) 2050037.
- [30] A.J. Power, L.J. Colling, N. Mead, L. Barnes, U. Goswami, Neural encoding of the speech envelope by children with developmental dyslexia, *Brain Lang.* 160 (2016) 1–10.
- [31] A.J. Power, N. Mead, L. Barnes, U. Goswami, Neural entrainment to rhythmic speech in children with developmental dyslexia, *Front. Human Neurosci.* 7 (2013) 777.
- [32] N. Molinaro, M. Lizarazu, M. Lallier, M. Bourguignon, M. Carreiras, Out-of-synchrony speech entrainment in developmental dyslexia, *Hum. Brain Mapp.* 37 (8) (2016) 2767–2783.
- [33] G.M. Di Liberto, V. Peter, M. Kalashnikova, U. Goswami, D. Burnham, E.C. Lalor, Atypical cortical entrainment to speech in the right hemisphere underpins phonemic deficits in dyslexia, *NeuroImage* 175 (2018) 70–79.
- [34] U. Goswami, A neural basis for phonological awareness? An oscillatory temporal-sampling perspective, *Curr. Dir. Psychol. Sci.* 27 (1) (2018) 56–63.
- [35] A.B.L. Tort, R. Komorowski, H. Eichenbaum, N. Kopell, Measuring phase-amplitude coupling between neuronal oscillations of different frequencies, *J. Neurophysiol.* 104 (2) (2010) 1195–1210.
- [36] A. Ortiz, F.J. Martínez-Murcia, J.L. Luque, A. Giménez, R. Morales-Ortega, J. Ortega, Dyslexia diagnosis by EEG temporal and spectral descriptors: an anomaly detection approach, *Int. J. Neural Syst.* 30 (07) (2020) 2050029.
- [37] D. Dvorak, A.A. Fenton, Toward a proper estimation of phase-amplitude coupling in neural oscillations, *J. Neurosci. Methods* 225 (2014) 42–56.
- [38] J. Aru, J. Aru, V. Priesemann, M. Wibral, L. Lana, G. Pipa, W. Singer, R. Vicente, Untangling cross-frequency coupling in neuroscience, *SI: Brain Rhythms and Dynamic Coordination, Curr. Opin. Neurobiol.* 31 (2015) 51–61.
- [39] R.T. Canolty, R.T. Knight, The functional role of cross-frequency coupling, *Trends Cogn. Sci.* 14 (11) (2010) 506–515.
- [40] R. van der Meij, M. Kahana, H. Maris, Phase-amplitude coupling in human electrocorticography is spatially distributed and phase diverse, *J. Neurosci.* 32 (1) (2012) 111–123.
- [41] M.J. Hülsemann, E. Naumann, B. Rasch, Quantification of phase-amplitude coupling in neuronal oscillations: comparison of phase-locking value, mean vector length, modulation index, and generalized-linear-modeling-cross-frequency-coupling, *Front. Neurosci.* 13 (2019).
- [42] A.B.L. Tort, M.A. Kramer, C. Thorn, D.J. Gibson, Y. Kubota, A.M. Graybiel, N.J. Kopell, Dynamic cross-frequency couplings of local field potential oscillations in rat striatum and hippocampus during performance of a T-maze task, *Proc. Natl. Acad. Sci.* 105 (51) (2008) 20517–20522.
- [43] S. Kullback, R.A. Leibler, On information and sufficiency, 1951.
- [44] J.M. Hurtado, L.L. Rubchinsky, K.A. Sigvardt, Statistical method for detection of phase-locking episodes in neural oscillations, *J. Neurophysiol.* 91 (4) (2004) 1883–1898.
- [45] E. Combrisson, T. Nest, A. Brovelli, R.A.A. Ince, J.L.P. Soto, A. Guillot, K. Jerbi, Tensorpac: an open-source python toolbox for tensor-based phase-amplitude coupling measurement in electrophysiological brain signals, in: D. Schneidman-Duhovny (Ed.), *PLoS Comput. Biol.* 16 (10) (2020) e1008302.
- [46] S. Boccaletti, V. Latora, Y. Moreno, M. Chavez, D.U. Hwang, Complex networks: structure and dynamics, *Phys. Rep.* 424 (4) (2006) 175–308.
- [47] D.J. Watts, S.H. Strogatz, Collective dynamics of 'small-world' networks, *Nature* 393 (6684) (1998) 440–442.
- [48] M.X. Cohen, *Analyzing neural time series data: theory and practice*, 2014.
- [49] P. Erdős, A. Rényi, On the evolution of random graphs, in: *The Structure And Dynamics Of Networks*, Princeton University Press, 2011, pp. 38–82.
- [50] M.D. Humphries, K. Gurney, Network 'small-world-ness': a quantitative method for determining canonical network equivalence, in: O. Sporns (Ed.), *PLoS One* 3 (4) (2008) e0002051.
- [51] S.H. Strogatz, Exploring complex networks, *Nature* 410 (6825) (2001) 268–276.
- [52] A. Réka, A.-L. Barabási, *Statistical Mechanics of Complex Networks*, Vol. 74, (1) 2002, pp. 47–97.
- [53] M.E.J. Newman, The structure and function of complex networks, *SIAM Rev.* 45 (2) (2003) 167–256.
- [54] A. Hagberg, P. Swart, D. S. Chult, *Exploring Network Structure, Dynamics, and Function Using Networkx*, Tech. Rep., LA-UR-08-05495; LA-UR-08-5495, Los Alamos National Lab. (LANL), Los Alamos, NM (United States), 2008.
- [55] C. Cortes, V. Vapnik, Support-vector networks, *Mach. Learn.* 20 (3) (1995) 273–297.
- [56] M. Ojala, G.C. Garriga, Permutation tests for studying classifier performance, in: *2009 Ninth IEEE International Conference On Data Mining, IEEE*, Miami Beach, FL, USA, 2009, pp. 908–913.
- [57] U. Goswami, A temporal sampling framework for developmental dyslexia, *Trends Cogn. Sci.* 15 (1) (2011) 3–10.
- [58] D. Poeppel, The neuroanatomic and neurophysiological infrastructure for speech and language, *SI: Communication and Language, Curr. Opin. Neurobiol.* 28 (2014) 142–149.
- [59] Z. Cui, Z. Xia, M. Su, H. Shu, G. Gong, Disrupted white matter connectivity underlying developmental dyslexia: A machine learning approach, *Hum. Brain Map.* 37 (2016).
- [60] P. Piorński, W. Gradkowski, I. Altarelli, K. Monzalvo, M. van Ermingen-Marbach, M. Grande, S. Heim, A. Marchewka, P. Bogorodzki, F. Ramus, K. Jednoróg, Multi-parameter machine learning approach to the neuroanatomical basis of developmental dyslexia: multi-parameter classification of dyslexic brain, *Hum. Brain Map.* 38 (2) (2017) 900–908.
- [61] A. Frid, L.M. Manevitz, Features and machine learning for correlating and classifying between brain areas and dyslexia, 2019, arXiv:1812.10622 [cs, q-bio, stat], arXiv:1812.10622.
- [62] H. Perera, M.F. Shiratuddin, K.W. Wong, K. Fullarton, EEG Signal analysis of writing and typing between adults with dyslexia and normal controls, *Int. J. Interact. Multimed. Artif. Intell.* 5 (1) (2018) 62.
- [63] Z. Rezvani, M. Zare, G. Žarić, M. Bonte, J. Tijms, M.W.V. der Molen, G.F. González, Machine learning classification of dyslexic children based on EEG local network features, 2019, bioRxiv, 569996, Cold Spring Harbor Laboratory.
- [64] A. Frid, Z. Breznitz, An SVM Based Algorithm for Analysis and Discrimination of Dyslexic Readers from Regular Readers Using ERPs, in: *2012 IEEE 27th Convention Of Electrical And Electronics Engineers In Israel*, 2012.
- [65] Y. García Chimenó, B. García Zapirain, I. Saralegui Prieto, B. Fernandez-Ruanova, Automatic classification of dyslexic children by applying machine learning to fMRI images, *Bio-Med. Mater. Eng.* 24 (6) (2014) 2995–3002.
- [66] S. Zahia, B. García-Zapirain, I. Saralegui, B.N. Fernandez-Ruanova, Dyslexia detection using 3D convolutional neural networks and functional magnetic resonance imaging, *Comput. Methods Programs Biomed.* 197 (2020) 105726.
- [67] A. Ortiz, P.J. López, J.L. Luque, F.J. Martínez-Murcia, D.A. Aquino-Britez, J. Ortega, An anomaly detection approach for dyslexia diagnosis using eeg signals, in: *Understanding The Brain Function And Emotions*, Springer, Cham, 2019, pp. 369–378.
- [68] F.J. Martínez-Murcia, A. Ortiz, J.M. Gorriç, J. Ramirez, P.J. Lopez-Abarejo, M. Lopez-Zamora, J.L. Luque, EEG Connectivity analysis using denoising autoencoders for the detection of dyslexia, *Int. J. Neural Syst.* 30 (07) (2020) 2050037.
- [69] F.J. Martínez-Murcia, A. Ortiz, R. Morales-Ortega, P.J. López, J.L. Luque, D. Castillo-Barnes, F. Segovia, I.A. Illan, J. Ortega, J. Ramirez, J.M. Gorriç, Periodogram connectivity of EEG signals for the detection of dyslexia, in: *Understanding The Brain Function And Emotions*, Springer, Cham, 2019, pp. 350–359.